Multi-Class Semantic Segmentation of Photovoltaic Module Defects and Features: Towards Industrial Robotic Applications

Shiva Hanifi[1 [0009−0001−9719−7342]], Sasan Jafarnejad[1 [0000−0003−2289−1425]], Mathieu Cormier[2 [0009−0004−2826−9869]], and Raphaël Frank[1 [0000−0001−8239−2041]]

[1] Interdisciplinary Centre for Security, Reliability and Trust, University of Luxembourg, 1855 Luxembourg City, Luxembourg
{shiva.hanifi, sasan.jafarnejad, raphael.frank}@uni.lu
[2] SolarCleano, 8346 Grass, Luxembourg
mc@solarcleano.com

Abstract. Automated defect detection in photovoltaic (PV) modules is essential for their maintenance and efficiency, yet challenges such as limited and imbalanced datasets hinder the adoption of high-accuracy systems. This study evaluates six semantic segmentation architectures based on U-Net and SegNet, paired with VGG16, MobileNet, and ResNet50 encoders, and trained on the 29-class dataset of PV module electroluminescence (EL) images. To address dataset imbalance, custom class weights were applied for all the *feature* and *defect* classes. VGG16-UNet outperformed other architectures, achieving a mean intersection over union (IoU) of 0.663 for *feature* classes and 0.326 across *defect* classes. In particular, it improved the detection of rare defects, such as *dead cell*, by 0.129 IoU. While previous research focused on a specific subset of classes, this study is the first to provide a comprehensive performance evaluation across all classes. It establishes a baseline for multi-class semantic segmentation in PV defect detection, laying the groundwork for further industrial applications such as in-field defect detection integrated into solar panel cleaning robots. Our implementation is publicly available at https://github.com/sntubix/pv-defect-segmentation, facilitating further research and development.

Keywords: Photovoltaic defects · Semantic segmentation · Electroluminescence imaging.

1 Introduction

Energy is central to addressing the climate crisis, serving as both a significant challenge and a key solution. Solar energy, the widely adopted renewable technology, accelerates clean energy transitions, fueling rapid expansion in solar photovoltaics (PV) [3]. This growth drives demand for efficient cleaning, monitoring, and maintenance of PV modules, the core components of PV systems. These

modules are prone to defects caused by aging and environmental factors, which reduce energy efficiency, shorten panel lifespan, and elevate operational costs. Advanced monitoring techniques, particularly imaging modalities such as electroluminescence (EL), have emerged as essential tools for detecting and localizing such degradation [15,19].

In this context, advancements in robotics and artificial intelligence (AI), particularly in computer vision (CV), increasingly align with PV system initiatives. The multidisciplinary capabilities of these technologies—providing precision, productivity, and intelligence—make them practical for manufacturing, installation, and inspection [12]. However, current CV-based defect detection approaches face critical bottlenecks, notably limited availability of large-scale, design-agnostic datasets encompassing diverse defect types. Moreover, the underrepresentation of specific defect categories results in severe dataset imbalances, limiting the generalization capability of trained deep learning models. As a consequence, fully automated, high-accuracy, in-field defect detection systems have not yet been widely adopted in industrial PV system practices [4,5,23].

This study presents our preliminary work on integrating CV-based defect detection into solar panel cleaning robots. In this initial phase, we utilize an existing dataset to train and evaluate semantic segmentation models for defect detection in electroluminescence (EL) images. To the best of our knowledge, this study is the first to comprehensively evaluate the performance on 29 distinct classes covering both *defect* and *feature* categories. An implementation of six semantic segmentation models is provided to ensure reproducibility and accessibility for future research, with the trained models establishing baselines for subsequent fine-tuning. By conducting a comprehensive evaluation across a diverse range of classes and progressing toward the development of a large-scale, design-agnostic dataset along with robust deep learning methodologies, this research addresses a critical gap in the automated maintenance and monitoring of photovoltaic modules.

The rest of the paper is organized as follows: Section 2 reviews the state-of-the-art advancements in datasets and deep learning architectures for PV module defect detection. Section 3 details the proposed methodology, and Section 4 presents a comprehensive quantitative and qualitative evaluation of our approach. Finally, Section 5 summarizes the key findings and explores promising directions for future research.

2 Related Work

This section provides an overview of prior research concerning two core aspects of CV-based PV module defect detection: datasets and deep learning architectures.

2.1 Datasets

Modern industrial defect detection utilizes imaging modalities such as electroluminescence (EL), photoluminescence (PL), infrared (IR), ultraviolet (UV), RGB,

and thermal imaging. Each modality differs in specifications, operational conditions, and suitability for specific PV cell types and defects [19,26]. Although several EL imaging datasets have recently emerged, large-scale, balanced datasets encompassing diverse defect types for all modalities remain scarce.

EL datasets are most prevalent, exhibiting significant variations in size and annotation types. The ELPV dataset, including 2,624 EL images and four defect classes, served as the first benchmark [2,4]. Its extension, E-ELPV, further expands the classification to five defect classes [6]. The SDLE dataset includes 1,028 EL images for classifying *good*, *cracked*, and *corroded* cells [27]. PVEL-AD provides 36,543 EL images with bounding box annotations for object detection [32]. The UCF dataset features 11,851 annotated EL images and 17,000 test images for segmenting ten defect classes [5]. The SCDD dataset is among the most comprehensive, encompassing 29 classes, 13 *features* corresponding to intrinsic components of the PV module design and 16 *defects* representing extrinsic faults. It includes segmentation masks for 765 EL images, sourced from a diverse range of PV module types [24].

Beyond EL datasets, the Infrared Solar Modules dataset comprises 20,000 low-resolution IR images for classification tasks, with 12 classes that include 11 anomaly types and one class for normal modules [20]. RGB images, widely used in aerial imaging for defect detection, lack comprehensive publicly available datasets. A notable exception is a global collection of solar installation images [26].

For the initial phase of this study, we selected the SCDD dataset to facilitate the training and evaluation of various deep learning architectures.

2.2 Deep-learning Architectures

Deep learning techniques have been widely applied for PV module defect detection in EL images, focusing on classification, object detection, and binary segmentation [8,9,25,33]. For multi-class semantic segmentation tasks, models such as U-Net [28] and SegNet [1] have demonstrated strong performance [13,18,24].

While earlier studies, such as [31] and [5], predominantly concentrated on a restricted subset of defect classes, the introduction of the SCDD dataset facilitated the investigation of a broader spectrum of classes. Pratt et al. in [24] have trained four models, including two U-Net variants, on a 24-class version of SCDD dataset. They have optimized and reported their model performances for a subset of the five most common defects (*crack, gridline, inactive*) and features (*ribbons, spacing*). SEiPV-Net [13], another model trained on SCDD, integrates Dense and Successive Features (DSF), Hierarchical Feature Precision and Extraction (HFPE), Contextual Characteristics Extraction and Attribute Fusion (CCEAF), and attention gate blocks to enhance segmentation accuracy. The same subset of most common classes is used for the evaluation and optimization of SEiPV-Net. Similarly, Attention-Based SegNet [18] combines a SegNet with a VGG16 [30] encoder and Convolutional Block Attention Module (CBAM) to enhance fine-grained segmentation, surpassing the performances reported in [24] and [13] on the same subset of classes.

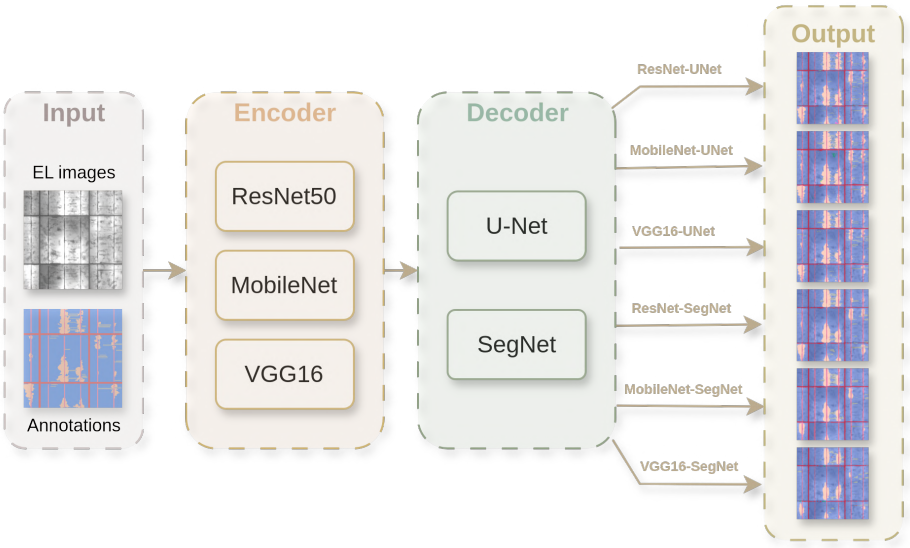

Fig. 1: Overview of the model architecture: Six models—ResNet50-UNet, MobileNet-UNet, VGG16-UNet, ResNet50-SegNet, MobileNet-SegNet, and VGG16-SegNet—trained on EL images and annotation masks from the SCDD dataset [24].

Emerging Directions: Semi-supervised and self-supervised learning techniques offer promising approaches to address the scarcity of large-scale annotated datasets [22]. The state-of-the-art includes studies employing self-supervised learning for solar panel segmentation and for solar cell classification [14,29]. A recent study applies momentum contrast-based self-supervised learning for module classification on the ELPV dataset, categorizing modules as *typical* or *irregular* [11]. Despite these developments, the application of such techniques to PV defect detection considering a wide range of defects remains largely unexplored, highlighting a significant opportunity for future research.

3 Methods

In this study, we prioritized multi-class semantic segmentation due to its ability to localize and quantify multiple classes within a single image, thereby preserving the maximum amount of information from EL images. We trained and evaluated six semantic segmentation architectures based on the U-Net and SegNet models, utilizing three distinct encoder backbones: VGG16, MobileNet, and ResNet50. This approach leveraged the unique strengths of each backbone in feature extraction, enabling a comparative analysis of their performance [1,7]. An overview of the employed architectures and the pipeline is provided in Fig. 1.

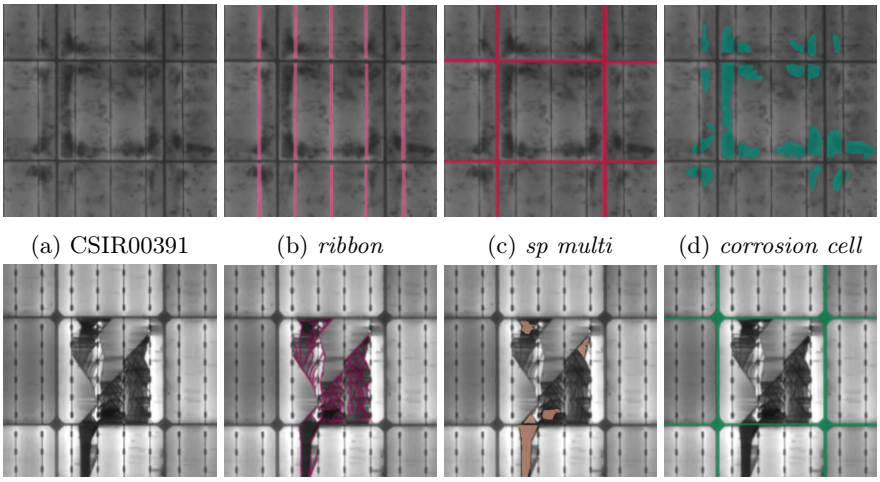

(a) CSIR00391 (b) *ribbon* (c) *sp multi* (d) *corrosion cell*

(e) CFVS00027 (f) *crack* (g) *inactive* (h) *sp mono*

Fig. 2: Representative ground truth annotations from the SCDD dataset [24]. The first row shows (a) EL image CSIR00391 with annotated features (*(b)ribbon*, *(c)sp multi*) and defect (*(d)corrosion*). The second row shows (e) EL image CFVS00027 with defects (*(f)crack*, *(g)inactive*) and feature (*(h)sp mono*).

We used the SCDD dataset [24] for model training, systematically restructuring it after a comprehensive pixel-count analysis of annotated classes. This restructuring aimed to achieve a balanced distribution of class samples across the training, validation, and test sets. However, certain underrepresented classes, such as *crack rbn edge, meas artifact* and *clamp*, were present in fewer than three images, making it infeasible to include samples from these classes in all dataset splits. All models were trained and evaluated using the modified SCDD dataset, comprising a total of 2204 augmented EL frames for training, 67 frames for validation, and 77 frames for testing, each accompanied by mask annotations corresponding to 16 classes of *defects* and 13 classes of *features*. A detailed description of all the classes within the SCDD dataset is available in [22]. In Fig. 2 we present two representative frames, showcasing a subset of six *feature* (*ribbon, sp multi, sp mono*) and *defect* classes (*corrosion, crack, inactive*).

The SCDD dataset exhibits significant class imbalance, with the number of pixels annotated for the *feature* category outnumbering those in the *defect* category by a factor of 40. Specifically, the most frequent *feature* class, *bckgnd*, contains 400,633,766 annotated pixels, whereas the least frequent *defect* class, *crack rbn edge*, comprises only 589 pixels. To address this challenge, we employed a weighted categorical cross-entropy loss function for model training. This approach incorporated class-specific weighting to ensure a more balanced representation of all semantic classes. The mathematical expression for the loss function is provided in Equation 1, where C denotes the total number of classes,

Table 1: Overview of 29 classes from the SCDD dataset [24], including annotated pixel counts and custom class weights to address the imbalance.

Feature	**Pixel Count**	**Class Weight**	**Defect**	**Pixel Count**	**Class Weight**
bckgnd	400,633,766	0.8	*gridline*	3,480,582	5.0
padding	129,806,535	0.7	*material*	2,847,203	4.0
ribbons	26,422,710	5.0	*edge dark*	2,639,518	3.0
border	13,219,690	2.0	*crack*	1,338,385	7.0
sp multi	12,917,390	3.0	*inactive*	1,173,418	5.0
sp mono	10,006,547	3.0	*brightening*	1,098,871	5.0
frame edge	5,470,904	2.0	*corrosion cell*	1,009,479	5.0
busbars	1,157,116	6.0	*corrosion rbn*	539,090	6.0
sp dogbone	675,711	6.0	*scuff*	291,468	6.0
sp mono halfcut	159,871	8.0	*splice*	224,002	7.0
text	40,250	4.0	*dead cell*	140,401	7.0
jbox	25,842	8.0	*belt mark*	117,387	6.0
clamp	4,952	4.0	*rings*	36,908	9.0
			star	34,739	7.0
			meas artifact	788	9.0
			crack rbn edge	589	10.0

and w_c represents the custom weight assigned to class c. The term $t_{i,c}$ refers to the true label for sample i and class c, which takes the value of 1 if the sample belongs to class c, and 0 otherwise. Additionally, $y_{i,c}$ represents the predicted probability for sample i and class c, and $\log(y_{i,c})$ is the natural logarithm of the predicted probability for class c.

$$L_i = -\sum_{c=0}^{C-1} w_c \cdot t_{i,c} \cdot \log(y_{i,c}) \tag{1}$$

The *defect* and *feature* classes, along with their respective annotated pixel counts and assigned class weights, are summarized in Table 1.

The assignment of class-specific custom weights was determined through a comprehensive analysis of prior work [13,17,24], and our experiments, considering three key factors: 1) Addressing the impact of class imbalance to ensure rare defects are not overlooked; 2) Enhancing detection accuracy for challenging defects while minimizing the risk of overfitting to more dominant or easily detectable classes; and 3) Prioritizing defects that are crucial to the performance and safety of PV modules. These factors were integral to optimizing the model's ability to detect critical defects effectively while maintaining generalization. Overall, as *feature* classes are more represented in the dataset, they have been assigned lower weights compared to *defect* classes.

All models were trained on an NVIDIA GeForce RTX 4090 GPU, using a batch size of 8. The Adam optimizer was used with a learning rate of 0.001. To ensure robust training and prevent overfitting, an early stopping was imple-

Table 2: Training and computational characteristics of segmentation models.

Model Architecture	Trainable Parameters	Epochs	Runtime
ResNet50-UNet	16,356,509	27	22m 54s
MobileNet-UNet	6,314,461	21	16m 21s
VGG16-UNet	12,336,605	30	27m 41s
ResNet-SegNet	14,845,085	30	24m 9s
MobileNet-SegNet	5,540,317	23	16m 58s
VGG16-SegNet	11,562,461	42	36m 31s

mented to monitor validation loss, with a patience parameter set to 10 epochs. Additionally, the steps per epoch parameter was calculated as the total number of input images divided by the batch size. Runtime information, the number of trainable parameters for each model, and the number of epochs they took to train considering the early stopping are reported in Table 2.

Finally, the models were evaluated across all 29 classes included in the dataset. Class-wise intersection over union (IoU) values, representing the overall IoU for each class, were computed for both *feature* and *defect* categories and are illustrated in Fig. 3. Model performance was further assessed regarding mean IoU for defects, features, and all classes. Additionally, frequency-weighted IoU, which accounts for class occurrence frequencies, was reported to provide a nuanced evaluation of model performance, particularly useful for imbalanced datasets like SCDD. Table 3 provides a comprehensive comparison of model performance including the above mentioned metrics.

4 Results

This section elaborates on the quantitative and qualitative evaluation of the trained models, with class-wise IoU serving as a representative metric for model performance comparison across all classes. A comprehensive comparison of class-wise IoU for both *defect* and *feature* classes across six segmentation models is visualized as heatmaps in Fig. 3. The results indicate that all models exhibit higher performance on *feature* classes compared to *defect* classes. This disparity in performance can be attributed to the more balanced representation of features in the training dataset and the greater consistency and homogeneity of their visual characteristics.

The *clamp* class was excluded from the performance evaluation presented in Fig. 3, as it was represented by a single image, which was included solely in the training set. Consequently, performance assessment for this class was not feasible. Moreover, the defect classes *crack rbn edge* and *meas artifact* remained undetected by all architectures, due to severe class imbalance that persisted despite the application of custom weighting. Addressing these challenges in future research will involve the collection of more balanced datasets and the application of advanced techniques, such as synsethic data generation.

Fig. 3: Class-wise IoU for (a) 16 *defects* and (b) 13 *features* reported for six models: ResNet50-UNet, MobileNet-UNet, VGG-UNet, ResNet50-SegNet, MobileNet-SegNet, and VGG-SegNe.

A compact quantitative comparison of the segmentation models based on mean IoU for *defects*, *features*, overall 29 classes, and frequency-weighted IoU is presented in Table 3. Regarding the encoder backbones, VGG16 emerged as the best-performing encoder, offering an optimal balance between deep feature extraction and fine-grained detail retention. Unlike ResNet50, VGG16 preserved spatial resolution by avoiding aggressive downsampling. Among decoders, UNet outperformed SegNet by effectively restoring fine details, utilizing learned upsampling, and achieving superior IoU scores. Overall, VGG16-UNet model achieved the best overall mean IoU of 0.494, with strong results in mean IoU for defects (0.326) and mean IoU for features (0.663), along with a high Frequency Weighted IoU (0.879). ResNet50-UNet is the second-best, with an overall mean IoU of 0.488, excelling in the mean IoU of features (0.681). In contrast, MobileNet-SegNet performed the worst with an overall mean IoU of 0.410 and lower values in both defect-related (0.254) and feature-related IoU (0.567).

Qualitative evaluation of the performance for all the models is presented in Fig. 4. A representative EL image from the SCDD test set, *CR01099*, is shown with its ground truth annotation and semantic segmentations from six models.

5 Conclusion and Future Work

This study marks the initial phase of our research on CV-based PV module defect detection with potential applications in industrial solar panel inspection robots.

Table 3: Comparison of segmentation models based on mean IoU for features, defects, overall 29 classes, and frequency-weighted IoU.

	UNet			SegNet		
	ResNet50	**MobileNet**	**VGG16**	**ResNet50**	**MobileNet**	**VGG16**
Mean IoU - Features	0.681	0.642	0.663	0.648	0.567	0.642
Mean IoU - Defects	0.295	0.261	0.326	0.294	0.254	0.288
Mean IoU - 29 classes	0.488	0.451	0.494	0.471	0.410	0.465
Freq. Weighted IoU	0.871	0.871	0.879	0.885	0.871	0.879

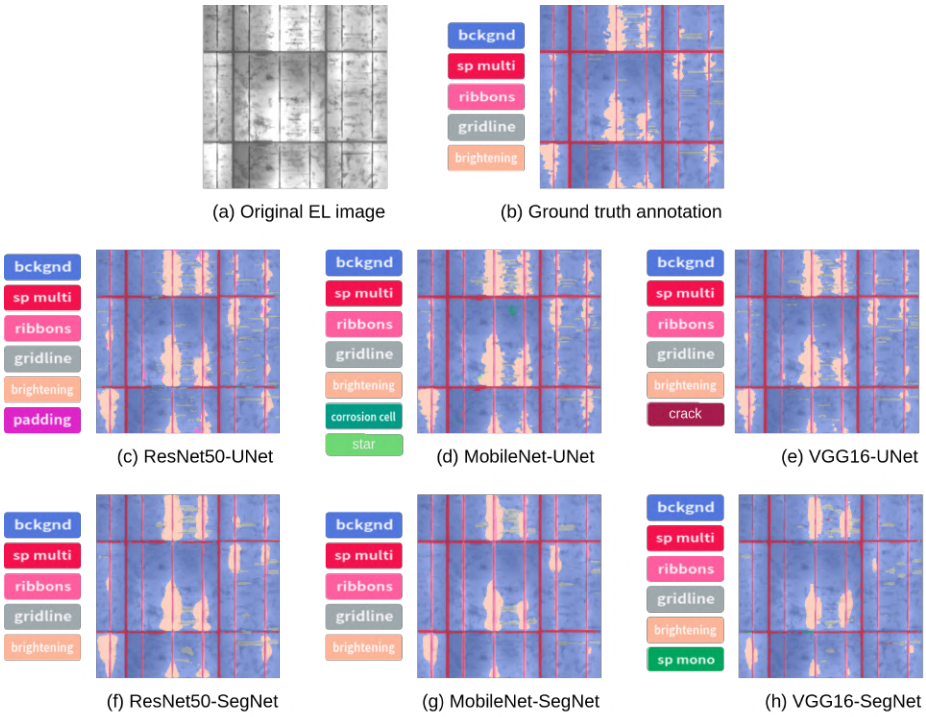

Fig. 4: Qualitative evaluation of segmentation models, showing ground truth annotation and model predictions for EL image CSIR01099 from the SCDD dataset [24].

We systematically trained and evaluated six U-Net and SegNet-style architectures, incorporating VGG16, MobileNet, and ResNet50 encoders, on the SCDD dataset comprising 29 defect classes. VGG16 emerged as the best-performing encoder, with its combination with UNet achieving the highest performance across evaluated metrics. To the best of our knowledge, this is the first comprehensive

analysis of model performance across all 29 *defect* and *feature* classes, accompanied by publicly available implementation code.

Building on these findings, this study outlines a threefold research focus to advance PV module defect detection. First, we will enhance synthetic data generation for underrepresented defect types [21] and integrate additional imaging modalities, including RGB and thermal imaging, to develop novel datasets. These non-invasive alternatives to EL imaging are particularly suited for field-deployed solar panels. Second, we aim to leverage existing EL datasets with diverse annotations for object detection and segmentation in hybrid architectures such as [16]. Lastly, we will implement Domain Adaptation techniques [10] to improve EL-informed feature detection on RGB images.

6 Acknowledgment

We acknowledge the financial support provided by SolarCleano Company[3] for this study.

References

1. Badrinarayanan, V., Kendall, A., Cipolla, R.: SegNet: A Deep Convolutional Encoder-Decoder Architecture for Image Segmentation. IEEE Transactions on Pattern Analysis and Machine Intelligence **39**(12), 2481–2495 (12 2017). https://doi.org/10.1109/TPAMI.2016.2644615
2. Buerhop-Lutz, C., Deitsch, S., Maier, A., Gallwitz, F., Berger, S., Doll, B., Hauch, J., Camus, C., Brabec, C.J.: A benchmark for visual identification of defective solar cells in electroluminescence imagery. In: 35th European PV Solar Energy Conference and Exhibition. pp. 1287–1289 (2018)
3. Chadly, A., Moawad, K., Salah, K., Omar, M., Mayyas, A.: State of global solar energy market: Overview, China's role, Challenges, and Opportunities (9 2024). https://doi.org/10.1016/j.horiz.2024.100108
4. Deitsch, S., Christlein, V., Berger, S., Buerhop-Lutz, C., Maier, A., Gallwitz, F., Riess, C.: Automatic classification of defective photovoltaic module cells in electroluminescence images. Solar Energy **185**, 455–468 (6 2019). https://doi.org/10.1016/J.SOLENER.2019.02.067
5. Fioresi, J., Colvin, D.J., Frota, R., Gupta, R., Li, M., Seigneur, H.P., Vyas, S., Oliveira, S., Shah, M., Davis, K.O.: Automated Defect Detection and Localization in Photovoltaic Cells Using Semantic Segmentation of Electroluminescence Images. IEEE Journal of Photovoltaics **12**(1), 53–61 (1 2022). https://doi.org/10.1109/JPHOTOV.2021.3131059
6. Grisanti, M., Spatafora, M.A.N., Ortis, A., Battiato, S.: E-ELPV: Extended ELPV Dataset for Accurate Solar Cells Defect Classification. Lecture Notes in Networks and Systems **822**, 837–848 (2024). https://doi.org/10.1007/978-3-031-47721-8{_}55, https://link.springer.com/chapter/10.1007/978-3-031-47721-8_55
7. Gupta, D.: Image Segmentation Keras : Implementation of Segnet, FCN, UNet, PSPNet and other models in Keras (7 2023), https://arxiv.org/abs/2307.13215v1

[3] https://solarcleano.com/en/

8. Henrique, R., Alves, F., Antero De Deus Júnior, G., Marra, E.G., Lemos, R.P.: Automatic fault classification in photovoltaic modules using Convolutional Neural Networks (2021). https://doi.org/10.1016/j.renene.2021.07.070, https://doi.org/10.1016/j.renene.2021.07.070
9. Hijjawi, U., Lakshminarayana, S., Xu, T., Piero, G., Fierro, M., Rahman, M.: A review of automated solar photovoltaic defect detection systems: Approaches, challenges, and future orientations. Solar Energy **266**, 112186 (2023). https://doi.org/10.1016/j.solener.2023.112186, http://creativecommons.org/licenses/by/4.0/
10. Hoyer, L., Dai, D., Van Gool, L.: DAFormer: Improving Network Architectures and Training Strategies for Domain-Adaptive Semantic Segmentation (11 2021), http://arxiv.org/abs/2111.14887
11. Huang, J., Arriffin, S.A., Chen, Y., Lin, J., Xu, W.: A Novel MoCo-Based Self-supervised Learning Framework for Solar Panel Defect Detection. IEEE Access pp. 1–1 (2025). https://doi.org/10.1109/ACCESS.2025.3529701, https://ieeexplore.ieee.org/document/10840178/
12. Iqbal, J., Al-Zahrani, A., Alharbi, S.A., Hashmi, A.: Robotics Inspired Renewable Energy Developments: Prospective Opportunities and Challenges. IEEE Access **7**, 174898–174923 (2019). https://doi.org/10.1109/ACCESS.2019.2957013
13. Joe, S..., Rehman, M.U.., Jang, Y.., Chong, K.T., Eesaar, H., Joe, S., Rehman, M.U., Jang, Y., Chong, K.T.: SEiPV-Net: An Efficient Deep Learning Framework for Autonomous Multi-Defect Segmentation in Electroluminescence Images of Solar Photovoltaic Modules. Energies 2023, Vol. 16, Page 7726 **16**(23), 7726 (11 2023). https://doi.org/10.3390/EN16237726, https://www.mdpi.com/1996-1073/16/23/7726/htmhttps://www.mdpi.com/1996-1073/16/23/7726
14. Kar, I., Mukhopadhyay, S., Ralte, Z.: Enhanced Solar Panel Multiclass Fine Grained Classification Using Attention Distilled Self-Supervised Learning and Combined Loss. 10th International Conference on Advanced Computing and Communication Systems, ICACCS 2024 pp. 133–139 (2024). https://doi.org/10.1109/ICACCS60874.2024.10717196
15. Köntges, M., Kurtz, S., Packard, C., Jahn, U., Berger, K.A., Kato, K., Friesen, T., Liu, H., Van Iseghem, M.: Review of Failures of Photovoltaic Modules (3 2014)
16. Li, F., Zhang, H., Xu, H., Liu, S., Zhang, L., Ni, L.M., Shum, H.Y.: Mask DINO: Towards A Unified Transformer-based Framework for Object Detection and Segmentation. Tech. rep., https://github.com/IDEA-
17. Mazen, F.M.A., Seoud, R.A.A., Shaker, Y.O.: Deep Learning for Automatic Defect Detection in PV Modules Using Electroluminescence Images. IEEE Access **11**, 57783–57795 (2023). https://doi.org/10.1109/ACCESS.2023.3284043
18. Mazen Ali Mazen, F., Shaker, Y.O., Ahmed Abul Seoud, R.: Attention-Based SegNet: Toward Refined Semantic Segmentation of PV Modules Defects. IEEE Access **12**, 100792–100804 (2024). https://doi.org/10.1109/ACCESS.2024.3431098
19. Maziuk, M., Jasińska, L., Domaradzki, J., Chodasewicz, P.: IMAGING METHODS OF DETECTING DEFECTS IN PHOTOVOLTAIC SOLAR CELLS AND MODULES: A SURVEY. Metrology and Measurement Systems **30**(3), 381–401 (2023). https://doi.org/10.24425/mms.2023.146426
20. Millendorf, M., Obropta, E., Vadhavkar, N.: INFRARED SOLAR MODULE DATASET FOR ANOMALY DETECTION https://github.com/RaptorMaps/
21. Paulin, G., Ivasic-Kos, M.: Review and analysis of synthetic dataset generation methods and techniques for application in computer vision. Artificial Intelligence Review **56**(9), 9221–9265 (9 2023). https://doi.org/10.1007/S10462-022-10358-3/FIGURES/10, https://link.springer.com/article/10.1007/s10462-022-10358-3

22. Pratt, L.: SOLAR CELL DEFECT DETECTION Deep Learning Models for Defect Detection in Electroluminescence Images of Solar PV Modules. Ph.D. thesis, University of the Witwatersrand (5 2024), https://wiredspace.wits.ac.za/items/188c94a9-0c1e-45f6-92b0-ca0cf6913e71
23. Pratt, L., Govender, D., Klein, R.: Defect detection and quantification in electroluminescence images of solar PV modules using U-net semantic segmentation. Renewable Energy **178**, 1211–1222 (11 2021). https://doi.org/10.1016/j.renene.2021.06.086
24. Pratt, L., Mattheus, J., Klein, R.: A benchmark dataset for defect detection and classification in electroluminescence images of PV modules using semantic segmentation. Systems and Soft Computing **5** (12 2023). https://doi.org/10.1016/j.sasc.2023.200048
25. Rahman, M.R.U., Chen, H.: Defects Inspection in Polycrystalline Solar Cells Electroluminescence Images Using Deep Learning. IEEE Access **8**, 40547–40558 (2020). https://doi.org/10.1109/ACCESS.2020.2976843
26. Rico Espinosa, A., Bressan, M., Giraldo, L.F.: Failure signature classification in solar photovoltaic plants using RGB images and convolutional neural networks. Renewable Energy **162**, 249–256 (12 2020). https://doi.org/10.1016/j.renene.2020.07.154
27. Roger H. French, Ahmad Maroof Karimi, Jennifer L Braid: Electroluminescent (EL) Image Dataset of PV Module Under Step-wise Damp Heat Exposures (2020). https://doi.org/10.17605/OSF.IO/4QRTV, osf.io/4qrtv
28. Ronneberger, O., Fischer, P., Brox, T.: U-Net: Convolutional Networks for Biomedical Image Segmentation. Lecture Notes in Computer Science (including subseries Lecture Notes in Artificial Intelligence and Lecture Notes in Bioinformatics) **9351**, 234–241 (2015). https://doi.org/10.1007/978-3-319-24574-4{_}28, https://link.springer.com/chapter/10.1007/978-3-319-24574-4_28
29. Sagaram, S., Didwania, K., Srivastava, L., Kasliwal, A., Kailas, P., Verma, U.: Solar Panel Segmentation :Self-Supervised Learning Solutions for Imperfect Datasets (2 2024). https://doi.org/10.3390/rs14215350, https://arxiv.org/abs/2402.12843v3
30. Simonyan, K., Zisserman, A.: Very Deep Convolutional Networks for Large-Scale Image Recognition. 3rd International Conference on Learning Representations, ICLR 2015 - Conference Track Proceedings (9 2014), https://arxiv.org/abs/1409.1556v6
31. Sovetkin, E., Achterberg, E.J., Weber, T., Pieters, B.E.: Encoder-Decoder Semantic Segmentation Models for Electroluminescence Images of Thin-Film Photovoltaic Modules. IEEE Journal of Photovoltaics **11**(2), 444–452 (3 2021). https://doi.org/10.1109/JPHOTOV.2020.3041240
32. Su, B., Zhou, Z., Chen, H.: PVEL-AD: A Large-Scale Open-World Dataset for Photovoltaic Cell Anomaly Detection. IEEE Transactions on Industrial Informatics **19**(1), 404–413 (1 2023). https://doi.org/10.1109/TII.2022.3162846
33. Tella, H., Mohandes, M., Liu, B., Rehman, S., Al-Shaikhi, A.: Deep Learning System for Defect Classification of Solar Panel Cells. 14th IEEE International Conference on Computational Intelligence and Communication Networks (2022). https://doi.org/10.1109/cicn.2022.77